Preparation and Mechanical Properties of Carbon Fiber Reinforced (BC$_x$–SiC)$_n$ Multilayered Matrix Composites

Wenbin Yang · Litong Zhang · Yongsheng Liu · Laifei Cheng · Weihua Zhang

Abstract A boron doped carbon materials (BC$_x$) was prepared by chemical vapor deposition and a 3D (BC$_x$–SiC)$_n$ multilayered matrix composite reinforced by carbon fiber, C/(BC$_x$–SiC)$_n$, was prepared by chemical vapor infiltration (CVI). XPS and SEM results showed that the BC$_x$ matrix had a boron content of 15 at.% and exhibited a very finely laminated structure. XRD analysis showed the BC$_x$ matrix was mainly carbon with B$_4$C crystals in it. SEM and EDS results showed that the BC$_x$ layers and the SiC layers were deposited within the interspaces of fiber bundles, alternately arranged and paralleled to each other as designed. The fracture energy of the composite was about 16.8 KJ m^{-2}. Flexural strength–displacement curve showed a remarkable metal-like yielding stage. Multiple fracture microstructures were induced by the multilayered matrix, such as delaminations of the multilayered matrix, deflections and propagations of cracks spread in the multilayered matrix layer by layer and long pullout of fiber bundles together with fiber clusters with multi-step pull-out structures. It was suggested that these special fracture behaviors absorbed a great deal of energy during the stress increasing and released the stress concentration, in this way, the toughness of the materials was improved.

Keywords Multilayered matrix composite · Boron doped carbon · Microstructure · Mechanical properties

1 Introduction

Continuous carbon fiber reinforced silicon carbide ceramic matrix composites (C/SiC) are promising candidates for many applications, particularly as aerospace and aircraft thermostructural components [1–6]. Nevertheless, a critical drawback of the C/SiC is the

W. Yang · L. Zhang (✉) · Y. Liu · L. Cheng · W. Zhang
National Key Laboratory of Thermalstructure Composite Materials,
Northwestern Polytechnical University, Xi'an, Shaanxi 710072, People's Republic of China
e-mail: wenbinyoung@mail.nwpu.edu.cn

poor oxidation resistance of the pyrocarbon interphase and carbon fibers, this limits long-term applications of C/SiC composite in high-temperature oxidizing environments [6–8].

Boron-containing materials, such as Boron [8], boron doped carbon (BC_x) [3–5, 9], and Si–B–C [10, 11] were widely used in coating, interphase and matrix, in order to form a glassy phase, which can seal the oxygen infiltration path then enhance the oxidation resistance. The coating systems could improve oxidation resistance significantly, while the durability was very limited because of the gasification of the glassy phase at high temperature and/or low pressure. The oxidation resistance of interphases was restricted by their thickness, if the cracks of matrix kept opening, the oxidation resistance of the interphases would not last long. The most promising way is to modify the SiC matrix by boron-containing materials [3–5, 10, 11]. A highly tailored multilayered matrix with the structure of ($BC_9/B_{13}C_2/(BC_9/SiC)$ sequences were prepared by Lamouroux [5] by means of pressure-pulsed CVI. It was proved that this multilayered matrix was tough and oxidation resistant. However, the structure of this multilayered matrix was too complicated to get. Besides the pressure-pulsed CVI, the ordinary CVI could also be employed to fabricate the multilayered matrix. Wu [9] has reported an oxidation protective multilayer CVD coating with the structure of ($SiC/B_{0.17}C_{0.83}/SiC$). It is proved that these multilayered coatings were very effective below 1,300°C.

In the present work, a multilayered matrix consists of (BC_x/SiC) sequences was prepared by CVI. Firstly, the morphologies and chemical compositions of the BC_x layer were characterized. Secondly, the microstructure and mechanical properties of the C/($SiC–BC_x$)$_n$ composites were analyzed. Finally, the relationship between the fracture microstructures and the fracture behaviors was discussed.

2 Experimental

2.1 Preparation of Samples

T-300 carbon fiber from Japan Toray was employed. The fiber preform was prepared using a four-step three dimension (4-step 3D) braiding method, and was by the Nanjing Institute of Glass Fiber, Nanjing Jiangsu, China. Low-pressure chemical vapor infiltration (LPCVI) process was used to deposit pyrolytic carbon (PyC) interphase, the SiC and BC_x matrix. The 0.2 μm PyC interphase was deposited for 120 h at 1,173 K and 5 kPa with C_3H_6. The BC_x matrix was deposited from BCl_3–C_3H_6–H_2 mixtures, the deposition temperature was 1,273 K, the pressure was 3 kPa, and the molar ratio of BCl_3 to C_3H_6 to H_2 was 1/1/5. Methyltrichlorosilane (MTS, CH_3SiCl_3) was used for the deposition of the SiC matrix. MTS vapor was carried by bubbling hydrogen. The conditions for deposition of SiC matrix were as follows: the deposition temperature was 1,273 K, the total pressure was 5 kPa, and the molar ratio of H_2 to MTS was 10. During the deposition of both SiC and BC_x, Argon with the same velocity of flow as H_2 was used as the dilute gas to get more uniform deposition.

T300 Carbon fiber bundles only deposited with BC_x were prepared for the purpose of characterizing of microstructure and chemical phase of the BC_x component.

The (BC_x–SiC)$_n$ multilayered matrix composite was prepared by following processing steps: firstly, about 0.2 μm PyC was deposited as interface; secondly, a layer of SiC was deposited; thirdly, a sequence of BC_x layer and SiC layer was deposited in turn; then the third step was repeated twice, namely $n=3$ in the form of (BC_x–SiC)$_n$. Finally, the composite was machined into the size of mechanical properties samples.
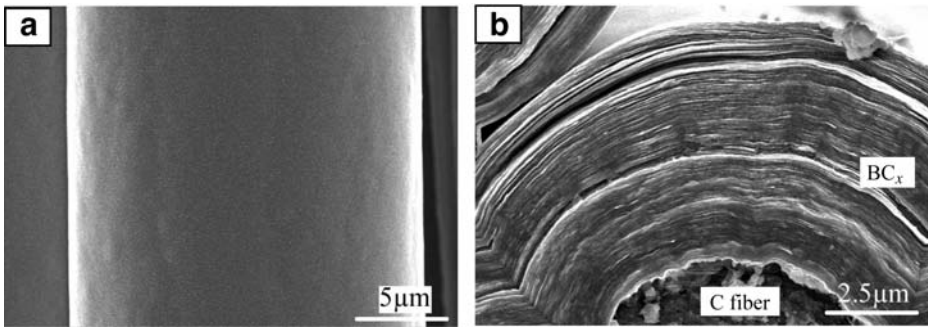
Fig. 1 Typical SEM images showing the morphology of BC_x materials deposited on the carbon fiber substrate at 1,273 K: **a** surface morphology and **b** tensile fracture morphology showing the finely laminated structure of BC_x

2.2 Measurements of the Composite

Cross-section micro-morphologies of the composite were observed with a scanning electron microscope (SEM, JSM-6700F). The cross-section was cut and polished carefully with diamond abrasive (W1) before analysis. An energy dispersive X-ray spectrum (EDS, EDXA) line scan was performed on the cross–section of the composite, to identify the presence of silicon, boron and carbon in the multilayered matrix. Phase identification was X-ray Photoelectron Spectroscopy (XPS) (AXIS ULTRA, KRATOS ANALYTICAL Ltd.) was both performed on the fiber bundle specimens. Phase identification was obtained with an X-ray diffraction device (XRD, Rigaku D/MAX-2400 with Cu Kà radiation). XPS was used to analyse the various bonds in which boron is involved. XPS analyses were performed using 1,486.71 eV monochromatic Al Kà radiation (15 kV, 10 mA). To compensate for surface charges effects, binding energies were calibrated using the C 1s hydrocarbon peak at 284.8 eV. The XPS peaks that used to analysis chemical bonds were collected without performing any etching of the surface to prevent the chemical bonds from being modified. The XPS peaks that used to determine the molar fraction of elements for the BC_x coating were collected after etching the surface for to eliminate of the adsorbent carbon and oxygen pollution.

Flexural strength of the composite specimens was measured by a three-point bending method at room temperature with samples of $3\times5\times40$ mm. The span dimension was 30 mm and the loading rate was 0.5 mm min^{-1}. Fracture toughness was measured by the single-edge notch beam method with samples of $3\times5\times40$ mm. The notch was produced by Electro-discharge machining with a depth and a width of 2.5 and 0.2 mm, respectively. The span dimension was 30 mm and the loading rate was 0.5 mm min^{-1}. The value of fracture toughness ($K1c$) was calculated by using of the American ASTME 399-74 expression,

$$K_{IC} = \sigma_C \sqrt{a}Y = \frac{P_C}{B}\frac{S}{W^{3/2}}f\left(C/W\right) \tag{1}$$

$$f(C/W) = 2.9\left(C/W\right)^{\frac{1}{2}} - 4.62.9\left(C/W\right)^{\frac{3}{2}} + 21.82.9\left(C/W\right)^{\frac{5}{2}} - 37.62.9\left(C/W\right)^{\frac{7}{2}} + 38.72.9\left(C/W\right)^{\frac{9}{2}} \tag{2}$$
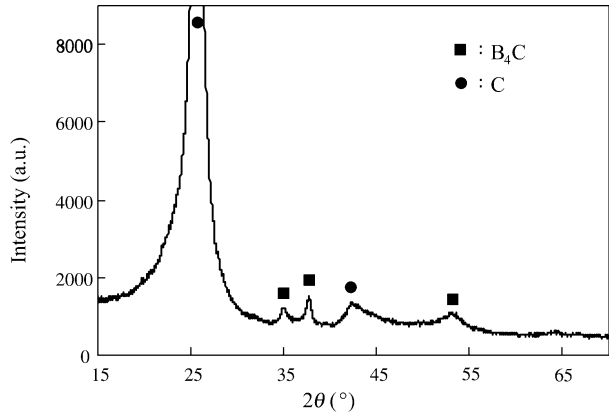
Where σ_c is the fracture load. Y is the geometrical factor for an edge crack in a three-point bend beam, calculated by Eq. 2. P_C is the fracture load; C is the notch depth; S is the span dimension, W and B are the thickness and broadness of the sample respectively.

3 Results and Discussion

3.1 Characterization of CVD BC_x Layer

Figure 1 showed the morphology of CVD BC_x materials deposited on the carbon fiber substrate (deposition time was 30 h). It was clear that the BC_x has a relatively smooth surface morphology and exhibits a finely laminated fracture structure with layers of nanometer distinction.

Figure 2 showed the XRD pattern of the BC_x materials. Two distinct peaks of carbon at 25.9°, 42.2°, and three small characteristic peaks of B_4C at 34.9, 37.8 and 53.4°, were respectively detected. This result indicated that the BC_x material in the multilayered matrix is a hybrid of carbon and B_4C crystal.

Table 1 listed molar fraction of elements for the BC_x measured by XPS analysis. The atom ratio of boron to carbon is about 15.01:82.66, namely $x \approx 5.5$ in the form of BC_x. By fitting the B 1s XPS spectrum, the proportions of B 1s components with different types of chemical states are achieved, as listed in Table 2. The components at 187.8 and 188.9 eV can be associated with a boron carbide such as B_4C and a boron atom included by substitution in the graphitic structure, as proposed by William et al. [12] and Jacques et al. [13]. The high energy components at 190.1, 191.8 and 193.0 eV correspond to boron atoms more and more oxidized, i.e. BC_2O at 190.0 eV, BCO_2 at 192.0 eV and B_2O_3 at 193.2 eV respectively. These results indicate that the deposited the BC_x was mainly boron atoms included by substitution in the graphitic structure.

Table 1 Molar fraction of elements (XPS) for the BC_x coating

Element	B	C	O
Content (at.%)	15.01	82.66	2.33

Table 2 Proportion of B 1s components (XPS) for the BC_x coating

Bonding structure	B_4C	B substituted in graphite lattice	BC_2O	BCO_2	B_2O_3
Binding energy/eV	187.9	189.0	190.1	191.8	193.0
Content in mole/at.%	11.0	42.8	28.3	10.0	7.8

3.2 Microstructure and Mechanical Properties of the Multilayered Matrix Composite

Figure 3 showed the cross-section morphology of the multilayered matrix composite. For the space between filaments was very limited, the first layer of SiC had nearly densified the fiber tows completely. Therefore, the multilayered matrix was mainly infiltrated among the fiber bundles. Figure 4 showed the cross section backscattered electron image and the EDS line scan in the bulk of the composite. The SiC layers (white area) and the BC_x layers (dark area) alternately arranged outside the fiber bundles and paralleled to each other as designed. Because the resolution is not high enough, these photographs have not distinguished the laminated structures shown in Fig. 1b.

From Figs. 3 and 4, it seemed that the multilayer matrix had less microcracks than C/SiC composites. However, some partial delaminations between the matrix layers could be observed in Figs. 3 and 4. Because the cross-section was cut and polished carefully, it was suggested that these matrix debondings were resulted from the residual thermal stress caused by coefficient of thermal expansion (CTE) mismatch among the carbon fibers, BC_x and SiC matrix.

Mechanical properties of the multilayered matrix composite were summarized in Table 3. The typical flexural strength–displacement curve was shown in Fig. 5. It was clear that the curve showed linearity before displacement value was less than 0.1 mm corresponding with the stress was under 200 MPa. After this short elastic stage the curve exhibited a remarkable metal-like yield stage, with the increasing of displacement, the slope of the curve gradually decreased until reached the peak stress (321 MPa). After the peak stress, instead of catastrophic fracture, the stress dropped slowly and consecutively. There were

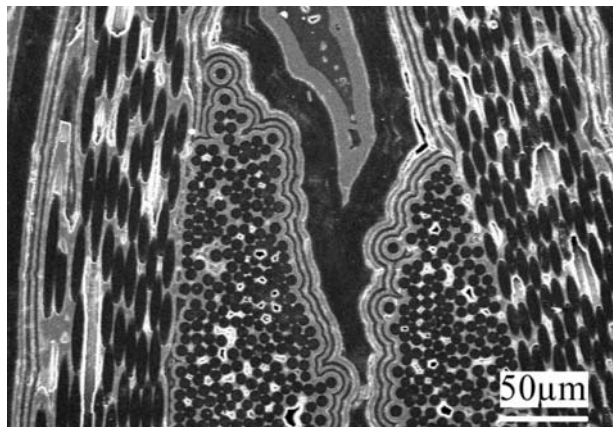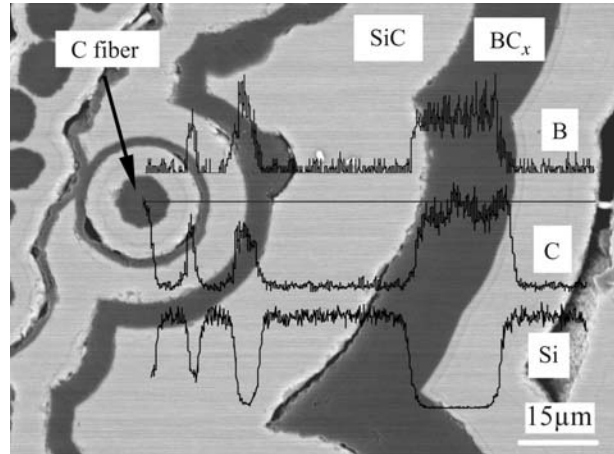**Fig. 3** Cross section micro-morphology of the 3D sample with multilayered matrix

two modes of stress decreasing showed in Fig. 5, one was low-amplitude fluctuation and consecutive decrease, and the other was step-like jump down.

Figure 6 showed the fracture microstructure of the flexural strength sample. In Fig. 6, there are long pullout of fiber bundles and fiber clusters. On the surface of fiber bundles, the multilayered matrix peeled off, also, some multi-step pull-out structures were detected at the end of the pulling out fiber clusters. Figure 7 showed a magnified view of micro-morphology of the multi-step pullout structure of the (BC$_x$–SiC) sequences matrix. Some delaminations within the multilayered matrix were also found in Fig. 7. Typical cracks spreading in matrix around fiber clusters was shown in Fig. 8. It was clearly that the crack was deflected into the direction along the multilayered matrix interfaces and propagated to next crack in the under layer matrix, then deflected and propagated in the same way again.

Figure 9 showed typical load–displacement curve of the fracture toughness with the samples that have been notched. The load–displacement curve has very similar metal-like characteristics as that showed in Fig. 5. The fracture toughness calculated from the Eq. 1 was 28.2 MPa m$^{1/2}$, which was higher than that of the 3D carbon fibers reinforced monolithic SiC matrix ceramic materials (C/SiC) prepared by Xu et al. [14] (20.3 MPa m$^{1/2}$) in the same method. Average work of fracture is 16.8 kJ·m$^{1/2}$, which was calculated as Xu did and also higher than the 3D carbon fibers reinforced monolithic SiC matrix ceramic materials (C/SiC) composite.

3.3 Discussion of the Fracture Behavior and Microstructure

With these typical microstructures, the metal-like flexural failure behavior of the composite can be qualitatively understood by damage and its accumulation resulted from the loading

Table 3 Mechanical properties of the multilayered matrix composites

Flexual strength (MPa)	Flexual modulus (GPa)	Fracture toughness (MPa m$^{1/2}$)	Work of fracture (KJ m^{-2})
321	62.8	28.2	16.8

Fig. 5 Typical flexural strength–displacement curve of the 3D $(BC_x–SiC)_n$ multilayered matrix composites
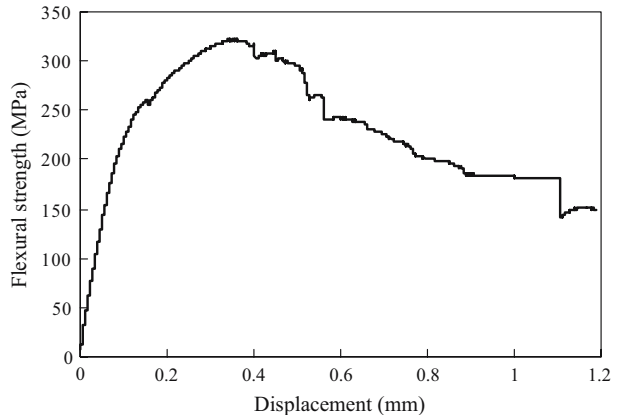
process. After the elastic stage, the matrix cracks induced by increasing stress begin to form and spread, then the crack tip reached the interfaces of the BC_x layers and SiC layers. Under the bending stress and the residual thermal stress mentioned above, the interfaces of the BC_x layers and SiC layers were prone to debond. In this case, it provided an easier path for cracks propagation, by which the length of crack diffraction and propagation was enhanced. Moreover, the interfacial friction occurred after interfaces' debond could stop cracks propagation through the matrix directly as usually observed in monotonic matrix. The cracks propagated from matrix to interfaces layer by layer with multiple cracks deflection as shown in Figs. 7 and 8. The typical multilayered matrix offered abundant chances for the cracks to deflect and propagate. A great deal of energy was absorbed by this way, the crack tip will be passivated and the stress concentration will be released, thus the tolerance to fractures of the composites was enhanced. When the cracks and delaminations accumulate to a limit, fibers began to bear the load, extend and rupture partially till pulled out in multiple modes such as filaments, clusters and fiber bundles. By this way, multiple small cracks propagation and matrix debonding prevented the composites from catastrophic failure and then enhanced their fracture toughness.

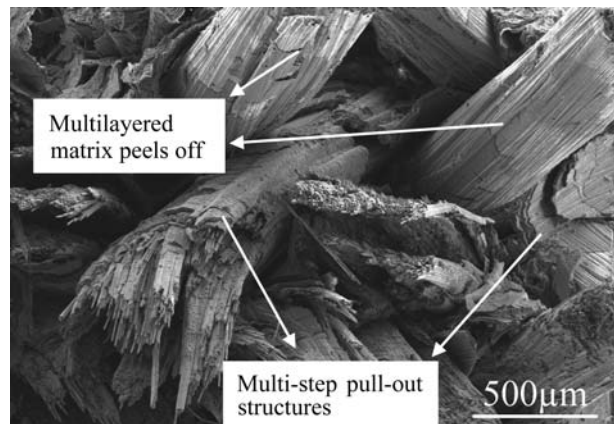Fig. 6 Facture morphology of the 3D $(BC_x–SiC)_n$ multilayered matrix composites

Fig. 7 Magnified view of micro-
morphology of the multi-step
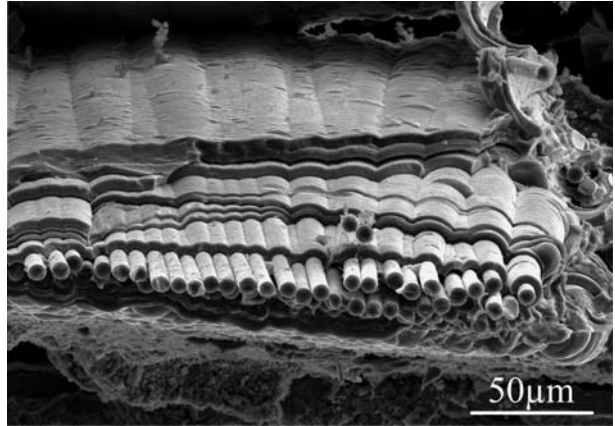pullout structure of the
$(BC_x–SiC)_n$ multilayered matrix

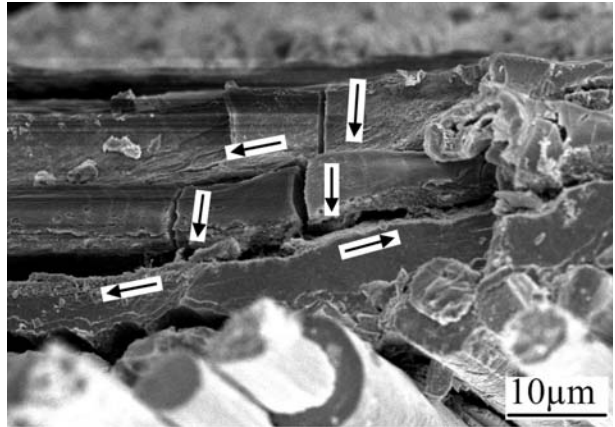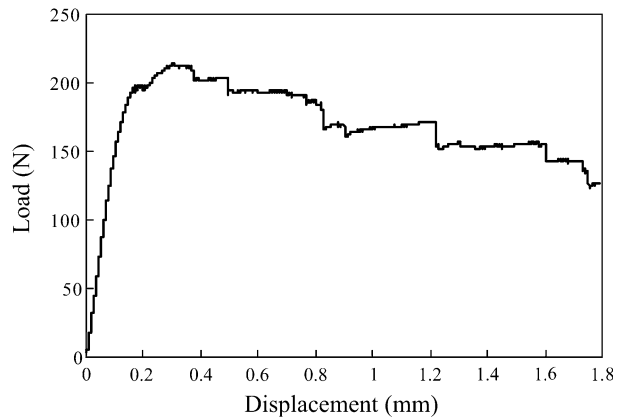**Fig. 8** Crack deflection and
propagation in the multilayered
matrix

Fig. 9 Typical load–displace-
ment curve of the notched 3D
$C/(BC_x–SiC)_n$ multilayered
matrix sample

It is supposed that the accumulation of cracks and delaminations was corresponded to the low-amplitude fluctuation and consecutive decrease in Figs. 5 and 9, while, the fiber bundles and groups pull-out were corresponded to the step-like jump down behavior in Figs. 5 and 9.

4 Conclusions

(1) A 3D $(BC_x–SiC)_n$ multilayered matrix composite reinforced by carbon fiber, $C/(BC_x–SiC)_n$, has been prepared by CVI. The BC_x layers and the SiC layers were deposited within the interspaces of fiber tows, alternately arranged and paralleled to each other as designed. The BC_x component had a boron content of 15.1 at.% and exhibited a very finely laminated fracture microstructure.

(2) Mean flexural strength of the multilayered matrix composite was about 321 MPa. The flexural strength–displacement curve exhibited a remarkable metal-like yield stage. Fracture toughness and work of fracture of the composite was about 28.2 MPa·m$^{1/2}$ and 16.8 KJ m^{-2}, respectively.

(3) Fracture microstructure of the flexural strength samples showed evident multiple failure modes as follows, delaminations of the multilayered matrix, deflections and propagations of cracks spread in the multilayered matrix layer by layer and long pullout of fiber bundles and fiber clusters with multi-step pull-out structures.

References

1. Schmidt, S., Beyer, H., Knabe, H., et al.: Advanced ceramic matrix composite materials for current and future propulsion technology applications. Acta Astronaut. **55**, 409–420 (2004)
2. Halbig, M.C., Brewer, D.N., Eckel A.J., et al.: Stressed oxidation of C–SiC composites (NASA/TM-1997-107457). NASA, New York (1997)
3. Naslain, R., Guette, A., Rebillat, F., et al.: Boron-bearing species in ceramic matrix composites for long-term aerospace applications. J. Solid State Chem. **177**, 449–456 (2004)
4. Naslain, R.: Design, preparation and properties of non-oxide CMCs for application in engines and nuclear reactors: an overview. Compos. Sci. Technol. **64**, 155–170 (2004)
5. Lamouroux, F., Bertrand, S., Pailler, R., et al.: Oxidation-resistant carbon-fiber-reinforced ceramic-matrix composites. Compos. Sci. Technol. **59**, 1073–1085 (1999)
6. Cutard, T., Huger, M., Fargeot, D., et al.: Ultrasonic characterization at high temperature of damage in ceramic composites subjected to tensile stresses. In: Naslain, R., (ed.) Proc. of HT-CMC1, pp. 33–49. Woodhead, Abington Cambridge (1993)
7. Lamouroux, F., Camus, G.J.: Oxidation effects on the mechanical properties of 2D woven C/SiC composites. J. Eur. Ceram. Soc. **14**, 177–188 (1994)
8. Liu, Y.S., Cheng, L.F., Zhang, L.T., Wu, S.J., et al.: Oxidation protection of multilayer CVD SiC/B/SiC coatings for 3D C/SiC composite. Mater. Sci. Eng. A. **466**, 172–177 (2007)
9. Wu, S.J., Cheng, L.F., Yang, W.B., et al.: Oxidation protective multilayer CVD SiC coatings modified by a graphitic B–C layer for 3D C/SiC composite. Appl. Compos. Mater. **13**, 397–406 (2006)
10. Quemard, L., Rebillat, F., Guette, A., Tawil, H., et al.: Self-healing mechanisms of a SiC fiber reinforced multi-layered ceramic matrix composite in high pressure steam environments. J. Eur. Ceram. Soc. **27**, 2085–2094 (2006)
11. Carrere, P., Lamon, J.: Creep behaviour of a SiC/Si–B–C composite with a self-healing multilayered matrix. J. Eur. Ceram. Soc. **23**, 1105–14 (2003)

12. William, C., Paulson, T.E., Onneby, C., Pantano, C.G.: Synthesis and characterization of boron-doped carbons. Carbon **33**, 367–374 (1995)
13. Jacques, S., Guette, A., Bodrrat, X., Langlais, F., et al.: LPCVD and characterization of boron-containing pyrocarbon materials. Carbon **34**, 1135–1143 (1996)
14. Xu, Y.D., Zhang, L.T., Cheng, L.F., Yin, H.F., Yin, X.W.: Mechanical properties of 3D fiber reinforced C/SiC composites Mater. Sci. Eng. **A 300**, 196–202 (2001)